

— *Supplemental Material* —
Controlled Self-Assembly of Periodic and Aperiodic Cluster Crystals

Kobi Barkan,¹ Michael Engel,² and Ron Lifshitz^{1,3}

¹*Raymond and Beverly Sackler School of Physics and Astronomy, Tel Aviv University, Tel Aviv 69978, Israel*

²*Department of Chemical Engineering, University of Michigan, Ann Arbor, MI 48109, USA*

³*Condensed Matter Physics 149-33, California Institute of Technology, Pasadena, CA 91125, USA*
(Dated: January 16, 2014)

Computational and theoretical methods, potential parameters, and additional figures supplementing the discussion in the main text.

DETERMINATION OF POTENTIAL PARAMETERS

The LP-Gaussian potential family is given in Fourier space by (Eq. (1) in the main text)

$$\tilde{U}(k) = e^{-\frac{k^2}{2\sigma^2}} (D_0 + D_2k^2 + D_4k^4 + D_6k^6 + D_8k^8). \quad (\text{S1})$$

The potential is self-dual in the sense that it has the same analytical form in real space (Eq. (2) in the main text),

$$\begin{aligned} U(r) &= \frac{1}{2\pi} \int_0^\infty \tilde{U}(k) J_0(kr) k dk \\ &= e^{-\frac{1}{2}\sigma^2 r^2} (C_0 + C_2r^2 + C_4r^4 + C_6r^6 + C_8r^8), \end{aligned} \quad (\text{S2})$$

where J_0 is the zeroth-order Bessel function and with

$$C_{2i} = \frac{1}{2\pi} \sum_{j=i}^4 (-1)^i \frac{2^{j-i}}{(j-i)!} \left(\frac{j!}{i!}\right)^2 D_{2j} \sigma^{2(i+j+1)}. \quad (\text{S3})$$

Given the desired values of the wavenumber ratio k_n , the Gaussian width σ , and the depth of the pair potential in reciprocal space \tilde{U}_{\min} , we run a Mathematica script to determine the coefficients $\{D_{2j}\}_{j=0}^4$ by simultaneously solving the following five equations:

$$\begin{aligned} U(0) = C_0 &= \frac{1}{2\pi} \sum_{j=0}^4 2^j j! D_{2j} \sigma^{2(j+1)} = 1, \\ \tilde{U}(1) = \tilde{U}(k_n) &= \tilde{U}_{\min}, \\ \left. \frac{d\tilde{U}}{dk} \right|_{k=1} &= \left. \frac{d\tilde{U}}{dk} \right|_{k=k_n} = 0. \end{aligned} \quad (\text{S4})$$

A substitution into the expressions for the coefficients $\{C_{2i}\}_{i=0}^4$ in Eq. (S3) and then into Eq. (S2) for the potential in real space completes the calculation. The values of σ are chosen so that the potentials are purely repulsive in real space, even though this is not required. All of the potential parameters used in this study are listed in Table S1.

COMPUTATIONAL METHODS

The main part of the simulations is performed with the HOOMD molecular dynamics (MD) simulation package [1] with either $N = 1024$ particles or $N = 16384$ particles in the NVT ensemble at mean densities $0.1 \leq \bar{c} \leq 2.0$. The interaction potential is cut off at $r = 10$, shifted and smoothed close to the cut-off to avoid truncation errors and discontinuities. Due to the relatively high density and the frequent particle overlap at our high densities, up to 500-1000 neighbors can be contained within the cut-off range, which is over an order of magnitude more than in typical (non-cluster) crystals with standard potentials (*e.g.* Lennard-Jones), slowing down the simulation. Total simulation times are 10^7 or 10^8 MD simulation steps, which means that typical simulation run times on a single GPU core are between a few hours and a few days. We verify the findings of all cluster crystals in several ways: (i) using NPT ensemble simulations; and (ii) repeating some of the simulations using a second MD package independent of HOOMD. Overall, we ran five simulations at each of the mean densities $\bar{c} \in \{0.1, 0.2, \dots, 2.0\}$ and for each of the five potentials—a total of 500 simulations.

Diffraction patterns were obtained using a Fast Fourier Transform of delta scatterers positioned at the centers of the particles. All observables (diffraction patterns, radial distribution functions, cluster sizes) were time averaged over 100 snapshots to minimize noise. The mean-field densities shown in Fig. 2 of the main text and in Fig. S6 below were obtained numerically by minimizing the mean-field free-energy, as described by BDL [2]. In order to obtain high resolution images more efficiently we also employed the method of Jiang and Zhang [3].

For performing the clustering operation, we first tested a naive clustering approach using a simple cut-off to join neighboring particles. However, this did not yield reliable results because in many cases clusters were either only partially detected or nearby clusters grouped together. Using the (still simple) DBSCAN algorithm [4] solved these problems. As discussed in the text, we always use a cluster size parameter $\text{MinPts} = 8$ and a variable cluster distance parameter that was adjusted to yield optimal results.

Potential parameter	Stripes	4-fold	6-fold	10-fold	12-fold
σ	0.784889	0.643467	0.714178	0.685894	0.770746
C_0	1	1	1	1	1
C_2	-1.11146	-0.72765	-0.875660	-0.794085	-1.09456
C_4	0.466920	0.193641	0.305132	0.252769	0.439744
C_6	-0.0552546	-0.0136926	-0.0283173	-0.0211568	-0.0492739
C_8	0.00217197	0.000324970	0.000889644	0.000601617	0.00183183
D_0	17.1419	22.8844	21.6032	23.0221	17.4524
D_2	-43.1030	-68.9652	-57.8779	-63.9132	-44.5109
D_4	35.4539	74.5064	52.9082	61.6601	37.5132
D_6	-10.7407	-34.4021	-19.2394	-24.3493	-11.8896
D_8	1.06780	5.70885	2.3966	3.34872	1.24928

TABLE S1. Potential parameters used in this study.

ADDITIONAL SIMULATION SNAPSHOTS

On the following pages, we include additional (mostly larger) simulation snapshots of the observed cluster crystals and their diffraction patterns. Note that all diffraction patterns show an inner set of sharp peaks, followed by a ring with little scattering, followed by a second ring of sharp peaks together with a broad ring of diffuse scattering. The diffuse scattering is caused by the particle disorder within the clusters.

- [1] J. A. Anderson, C. D. Lorenz, and A. Travasset, *J. Comp. Phys.* **227**, 5342 (2008). HOOMD-blue web page: <http://codeblue.umich.edu/hoomd-blue>.
- [2] K. Barkan, H. Diamant, and R. Lifshitz, *Phys. Rev. B* **83**, 172201 (2011).
- [3] K. Jiang and P. Zhang, *J. Comput. Phys.* **256**, 428 (2014).
- [4] M. Ester, H.-P. Kriegel, J. Sander, and X. Xu, in *Proceedings of the Second International Conference on Knowledge Discovery and Data Mining*, edited by E. Simoudis, J. Han, and U. M. Fayyad (1996) pp. 226–231.

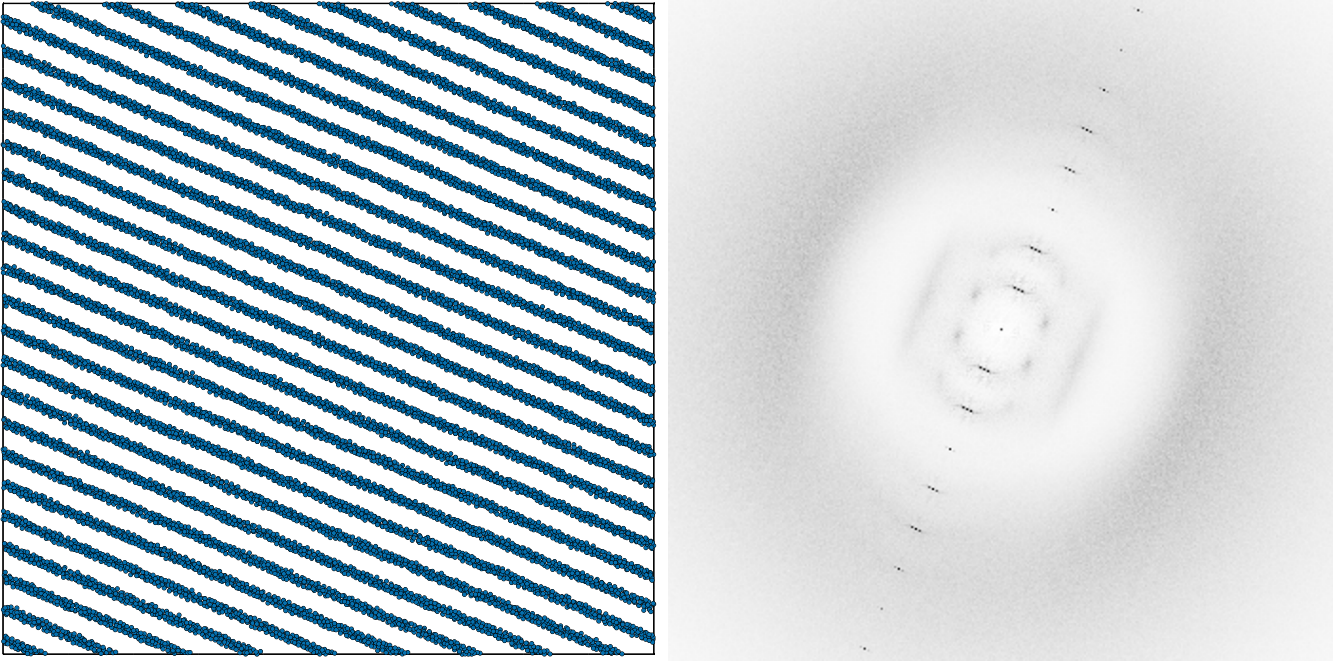


FIG. S1. Lamellar pattern formed from particles aligning into parallel stripes. Particles are still highly mobile within the stripes. Simulation parameters: $N = 16384$, $\bar{c} = 0.9$, $T = 0.03$.

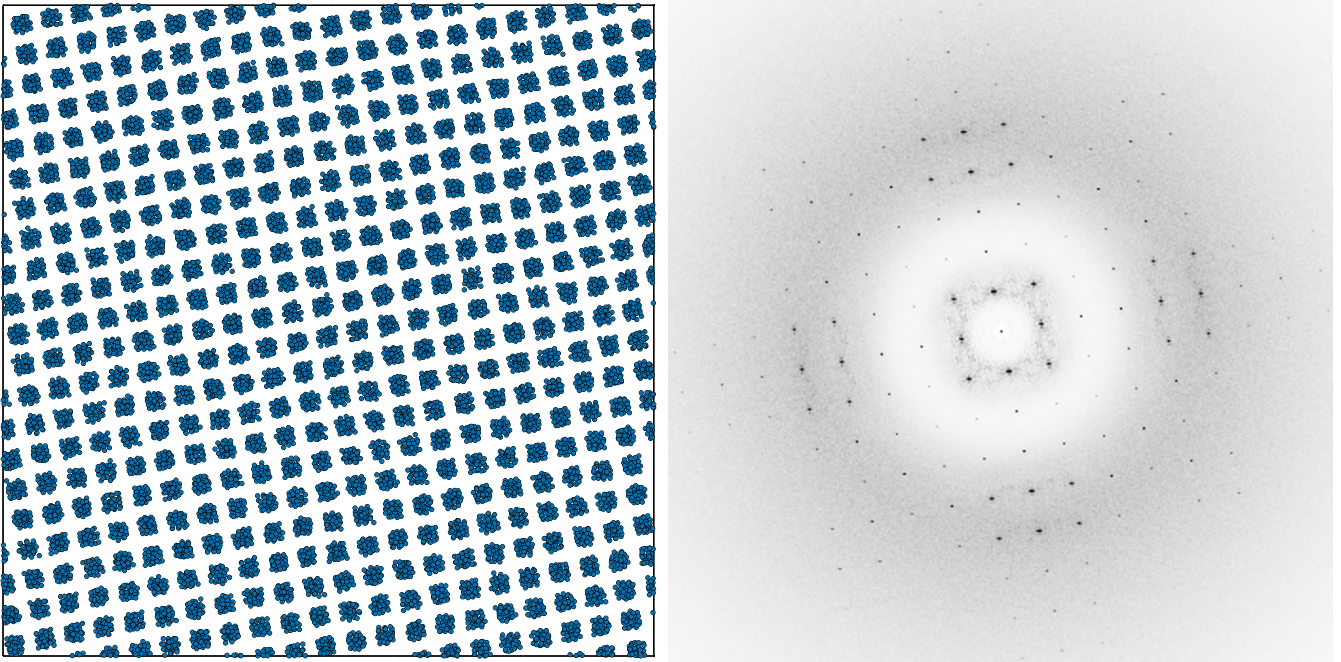


FIG. S2. Periodic 4-fold cluster crystal forming a square lattice. Simulation parameters: $N = 16384$, $\bar{c} = 0.9$, $T = 0.03$.

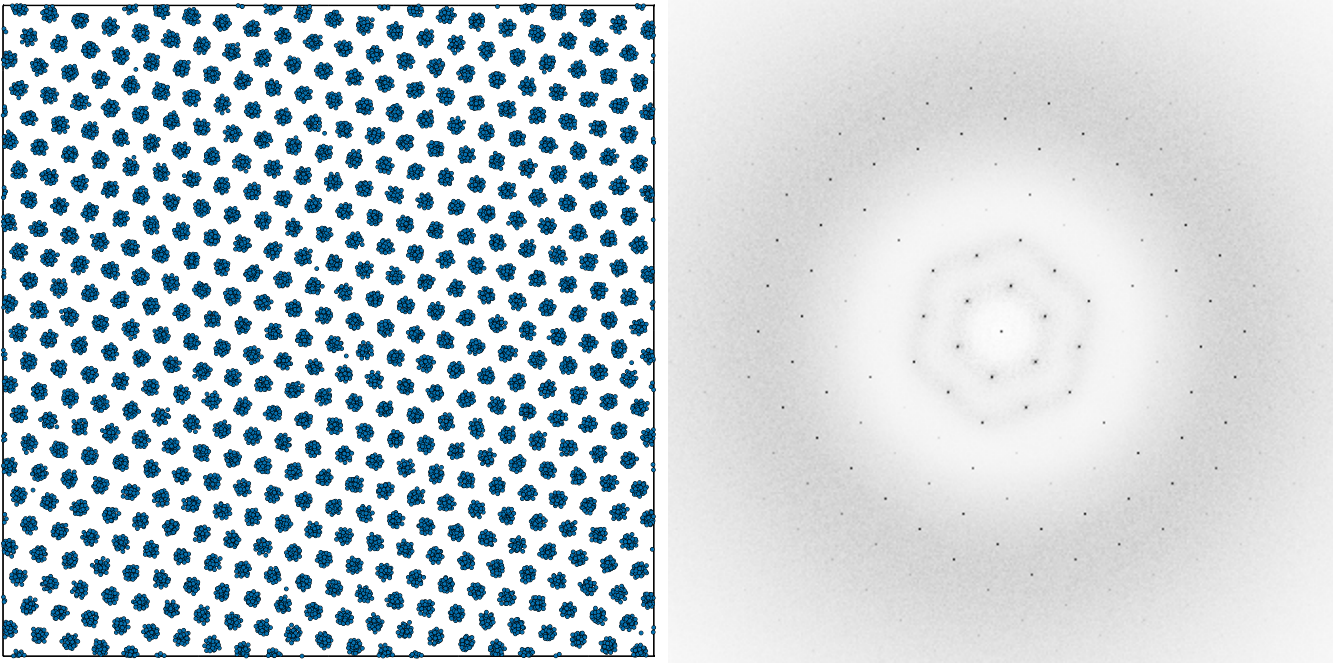


FIG. S3. Periodic 6-fold cluster crystal forming a triangular lattice. Simulation parameters: $N = 16384$, $\bar{c} = 0.7$, $T = 0.03$. Note how a few single-particle “clusters” seem to be caught at the centers of large-cluster triangles. At higher densities, these proliferate to form a superlattice structure, as can be seen in Fig. S6.

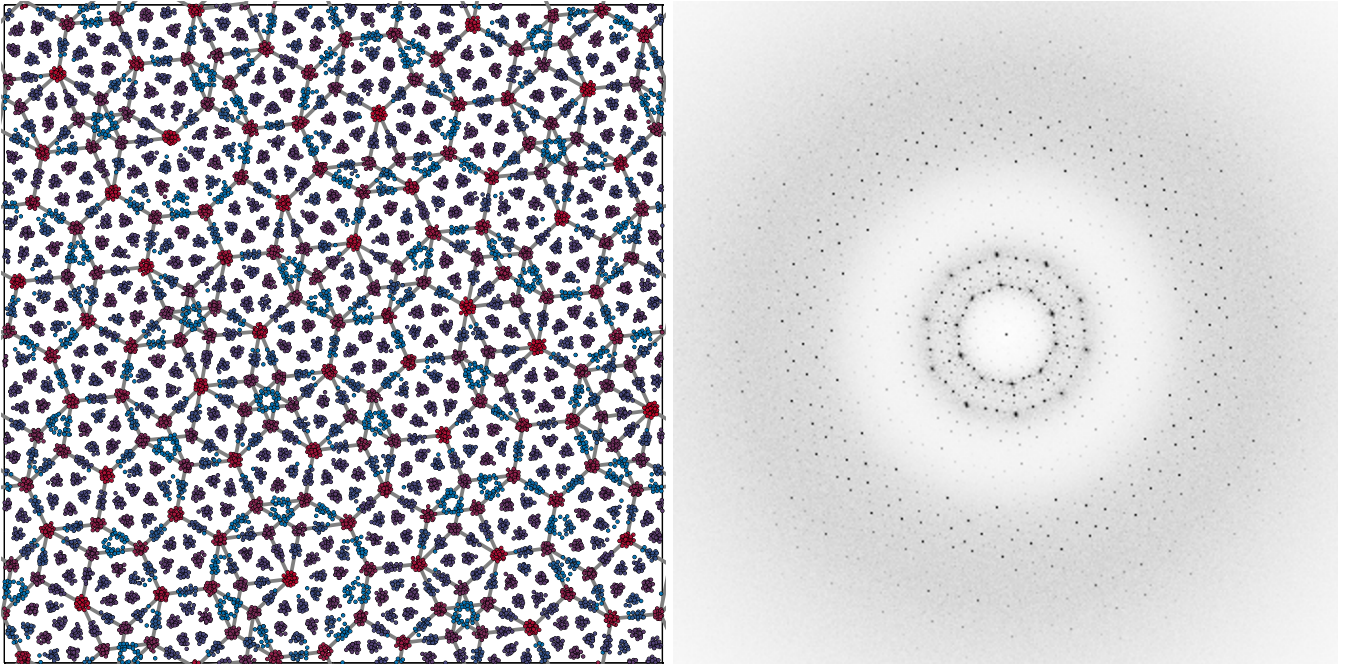


FIG. S4. Quasiperiodic 10-fold cluster crystal forming a pentagon Penrose (P1) tiling with some phason disorder. Simulation parameters: $N = 16384$, $\bar{c} = 0.6$, $T = 0.03$. Clusters are identified and colored according to their size from small (blue, size ≤ 10) to large (red, size ≥ 30). Second-nearest-neighbor clusters of size ≥ 19 are connected by bonds to obtain the tiling.

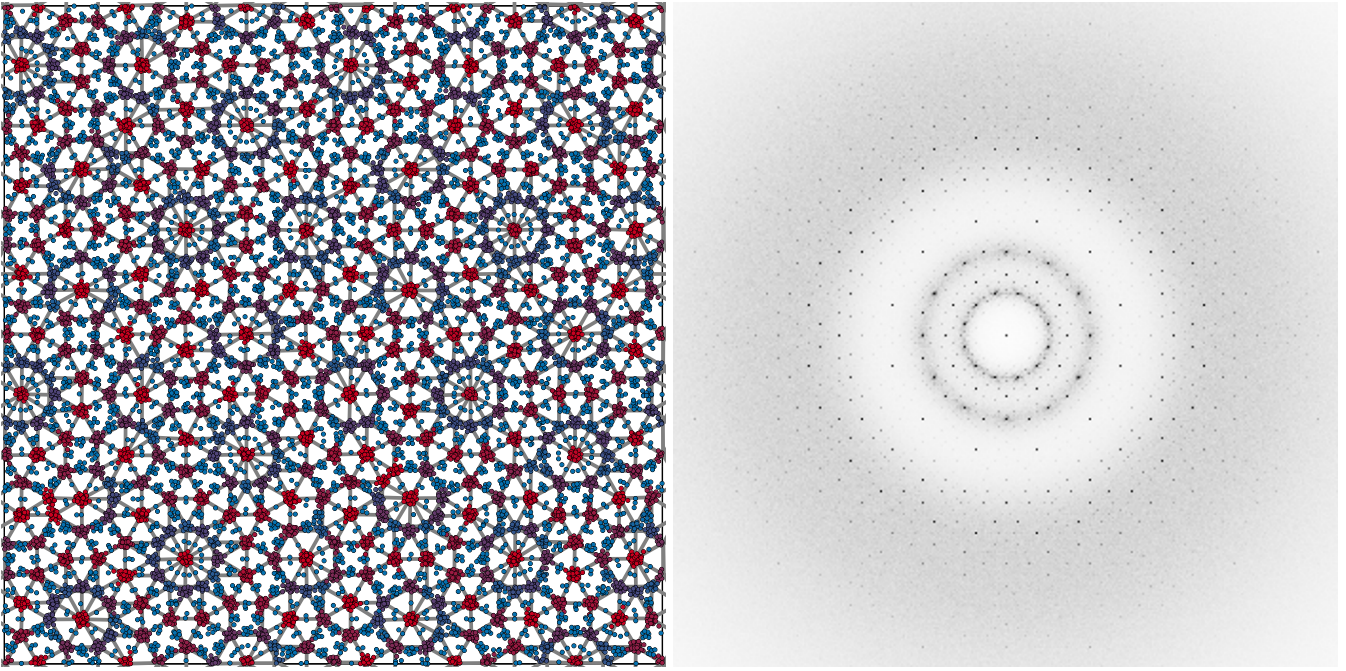


FIG. S5. Quasiperiodic 12-fold cluster crystal forming a square-triangle-rhombus tiling with some phason disorder. Simulation parameters: $N = 16384$, $\bar{c} = 0.8$, $T = 0.03$. Clusters are identified and colored according to their size from small (blue, size ≤ 10) to large (red, size ≥ 30). Second-nearest-neighbor clusters of size ≥ 10 are connected by bonds.

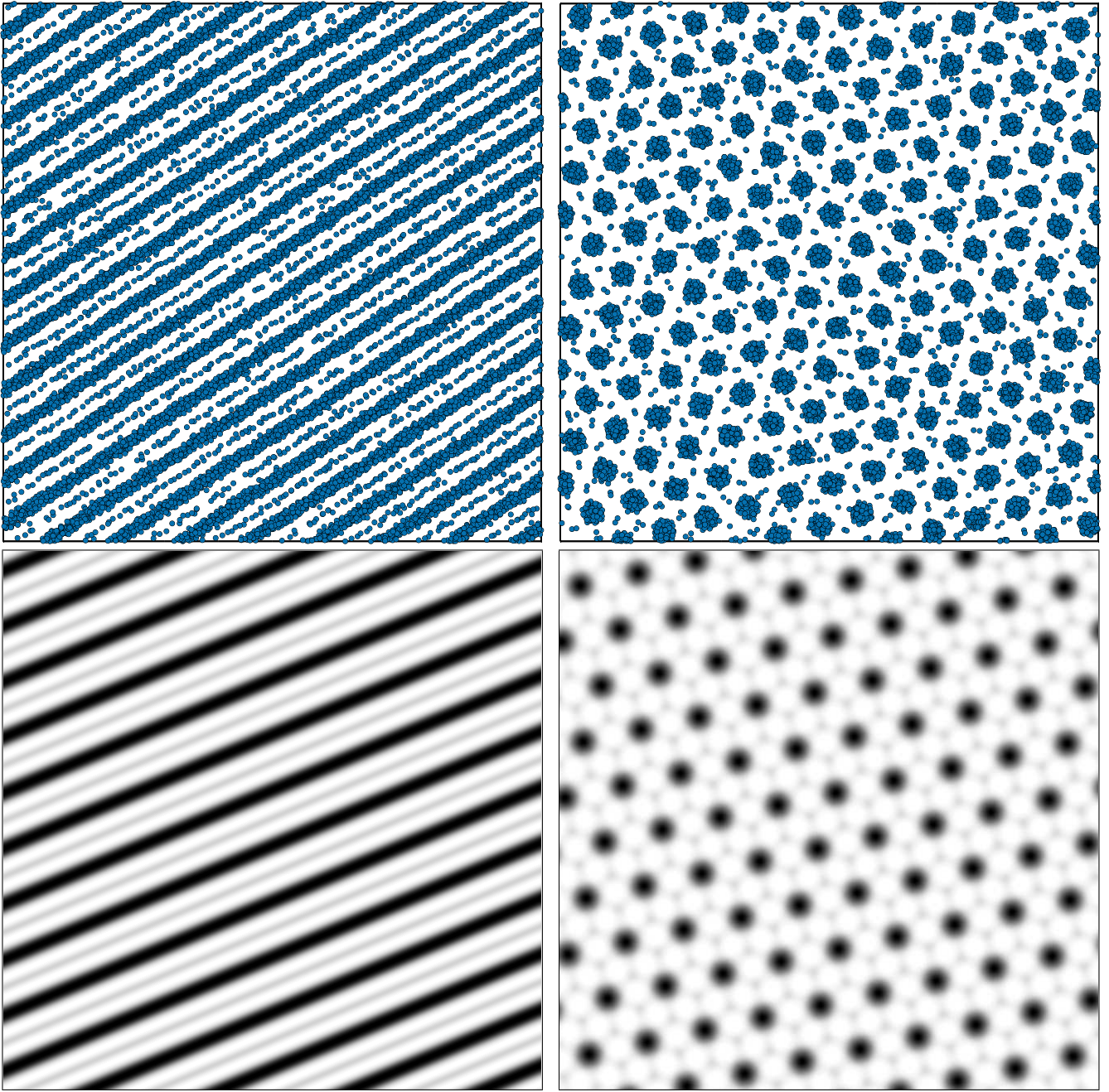


FIG. S6. Confirmation of superstructures of secondary lamellae and secondary clusters, as predicted by the mean-field results. At sufficiently high density and temperature (close to melting) secondary lower-density lamellae and clusters appear in the striped phase (left column) and the hexagonal phase (right column), respectively. Top row: Simulation snapshots at density $\bar{c} = 2.0$, the highest density studied in this work, and at temperatures close to melting. To decrease noise, these snapshots are rapidly cooled to $T = 0.1$ (2-fold, left) and $T = 0.06$ (6-fold, right). Bottom row: The secondary superstructures as observed in the mean-field calculations. The mean field results shown here are identical to the insets in Fig. 2 of the main text.

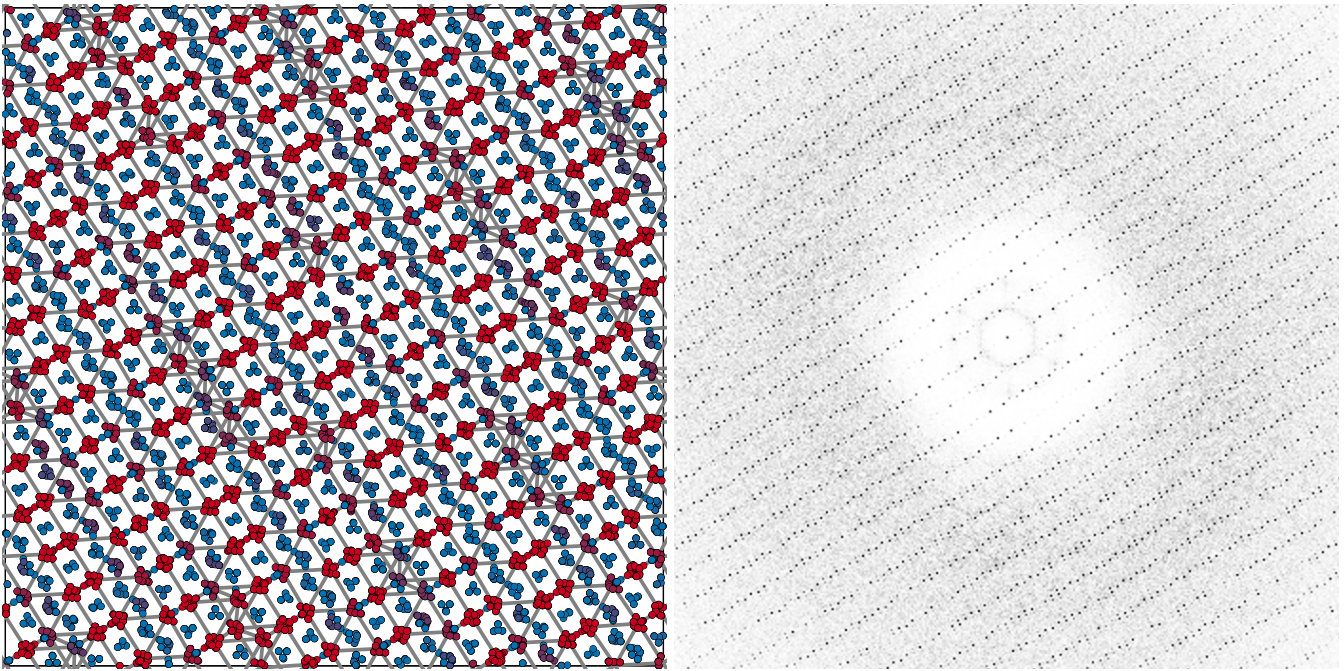


FIG. S7. An incomplete transformation of the 12-fold quasicrystal into a compressed hexagonal phase observed at low temperature. Simulation parameters: $N = 16384$, $\bar{c} = 1.9$, $T = 10^{-3}$. Clusters are identified and colored according to their size from small (blue, size ≤ 10) to large (red, size ≥ 30). Second-nearest-neighbor clusters of size ≥ 20 are connected by bonds. The tiling consists of alternating rows of two types of compressed hexagonal tiles, each consisting of a pair of triangles connected by either one rectangle or two.

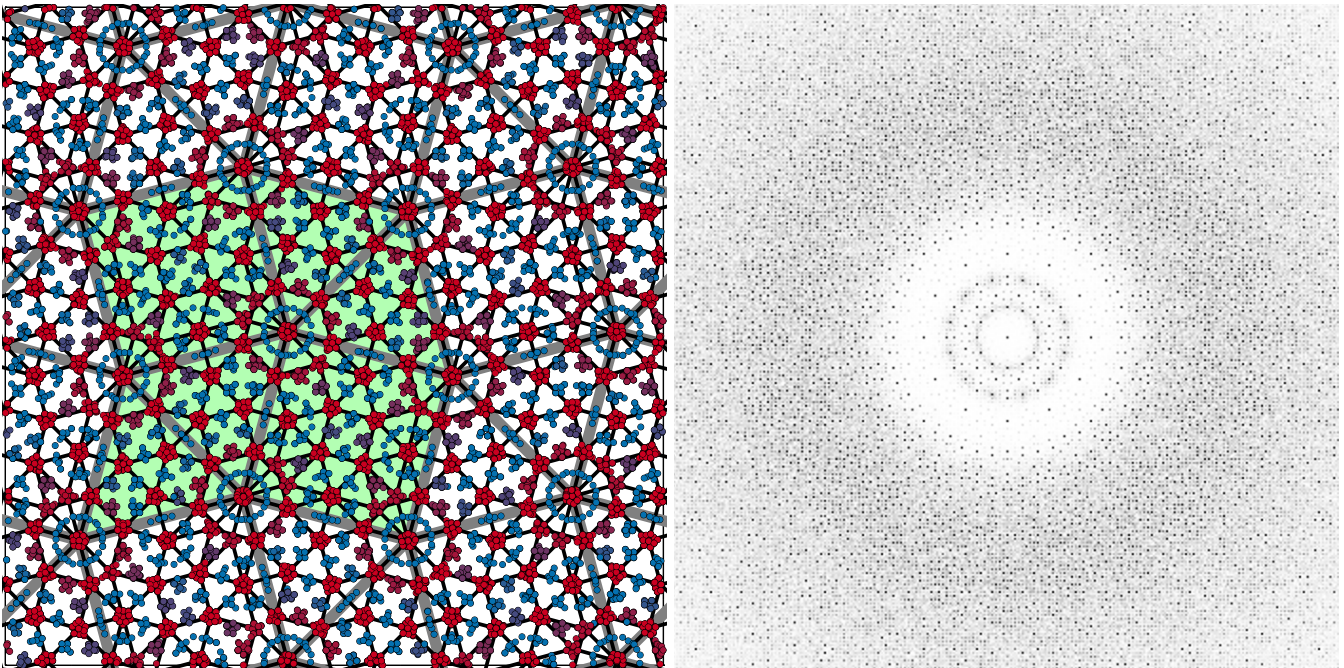


FIG. S8. A σ -phase approximant of the 12-fold quasicrystal observed at low temperature. Simulation parameters: $N = 16384$, $\bar{c} = 1.6$, $T = 10^{-3}$. Clusters are identified and colored according to their size from small (blue, size ≤ 10) to large (red, size ≥ 30). Second-nearest-neighbor clusters of size ≥ 10 are connected by black bonds, revealing square, triangular, and rhombic tiles that are the same building blocks for the dodecagonal quasicrystal shown in Fig. S5. Larger clusters (of size ≥ 45), located at the centers of 12-fold rings, are connected by thick gray bonds, revealing the σ -phase approximant, where each vertex is surrounded by a pair of triangles followed by a square, another triangle, and another square, commonly denoted as $3^2.4.3.4$. The unit cell of the approximant (four large triangles and two large squares) is highlighted green. Note the pseudo-12-fold diffraction diagram, and compare with the one in Fig. S5.